CrystEngComm

PAPER

View Article Online
View Journal | View Issue

Cite this: *CrystEngComm*, 2016, **18**, 1446

In situ synthesis of porous ZnO-embedded $Zn_{1-x}Cd_xS$/CdS heterostructures for enhanced photocatalytic activity†

Rong Chen, Kui Li, Xiao-Shu Zhu, Shuai-Lei Xie, Long-Zhang Dong, Shun-Li Li* and Ya-Qian Lan*

Received 10th December 2015,
Accepted 20th January 2016

DOI: 10.1039/c5ce02420j

www.rsc.org/crystengcomm

The *in situ* synthesis of ZnO-embedded $Zn_{1-x}Cd_xS$/CdS heterostructure nanocrystals was achieved by using a simple surfactant-free hydrothermal route. The morphology and the exposed active site content of $Zn_{1-x}Cd_xS$/CdS could be facilely modulated by varying the particle size of ZnS precursors, and the heterostructure with the smallest particle size showed the highest photocatalytic activity of 22.99 mmol h^{-1} g^{-1} in Na_2S + Na_2SO_3 solution. Furthermore, the *in situ* embedding of the ZnO cocatalyst on the $Zn_{1-x}Cd_xS$/CdS heterostructure dramatically improved its photocatalytic activity to 84.17 mmol h^{-1} g^{-1}, which is 765 times higher than that of CdS prepared by a hydrothermal method. More significantly, the ZnO-embedded $Zn_{1-x}Cd_xS$/CdS heterostructure gave a considerable H_2 production rate even in the absence of hole scavengers, whereas the bare $Zn_{1-x}Cd_xS$/CdS exhibited no hydrogen evolution, and it showed very competitive photocatalytic activity in methanol in comparison with that in Na_2S + Na_2SO_3 solution under similar alkaline circumstances. These investigations indicate that the existence of the ZnO cocatalyst in the heterostructure could not only effectively improve the photocatalytic activity by suppressing the recombination of charge carriers and acting as a photocatalytic reaction site, but also make it possible to adopt methanol as the sacrificial reagent for sulfide photocatalysts.

Introduction

Semiconductor nanocrystals have attracted much attention in the areas of photocatalysis[1] and photoelectrochemistry (PEC)[2] due to their excellent photocatalytic and photoelectronic properties.[3] However, the limited visible light absorption and rapid recombination of photo-generated charge carriers in semiconductor photocatalysts restrict their practical applications.[4] Fabricating sulfide heterostructures not only facilitates the separation of charge carriers,[5] but also improves the visible light absorption due to their narrow band gap.[6] However, the preparation of sulfide heterostructures usually involves complex routes including loading one semiconductor onto the other one, which needs precise control of synthetic parameters in each step.[7] This method not only limits the scale-up synthesis of heterostructures,[5] but also induces the formation of interfacial problems.[8] Moreover, the surface-based characteristic of the photocatalytic water splitting reaction makes the exposed active site content an important factor for the design of high-performance heterostructure photocatalysts. Organic surfactants were extensively adopted to modulate the morphology of the nanomaterials. However, the surfactants inevitably contaminate the heterostructures and may substantially impair the performance of the heterostructures.[9] Therefore, searching for an efficient surfactant-free hydrothermal method for the *in situ* synthesis of sulfide heterostructures with improved amounts of active sites is an important subject from both theoretical and practical viewpoints.

Cocatalysts such as graphene, Pt, NiO and MoS_2 could facilitate the separation of photo-excited hole/electron pairs and/or act as H_2-production sites.[10] ZnO has been widely used as a photocatalyst due to its high electron mobility and long photo-excitation lifetime.[11] Notably, it was extensively demonstrated that the oxygen vacancies in ZnO could work as electron traps to accept electrons and inhibit the recombination of charge carriers.[12] The oxygen vacancies in ZnO could also act as the favored sites for catalyzing the *N*-formylation reaction as reported by Zhu's group.[13] Furthermore, it was demonstrated in Zong's investigation that ZnO could function as a cocatalyst for improving the catalytic activity in the combined reforming–hydrogenolysis of glycerol.[14] These unique features of ZnO make it an excellent cocatalyst for

Jiangsu Key Laboratory of Biofunctional Materials, College of Chemistry and Materials Science, Nanjing Normal University, Nanjing 210023, PR China. E-mail: yqlan@njnu.edu.cn, slli@njnu.edu.cn

† Electronic supplementary information (ESI) available: Figures and tables. See DOI: 10.1039/c5ce02420j

improving the photocatalytic activity of sulfide photocatalysts. On the other hand, it is well known that sulfide photocatalysts show excellent photocatalytic activity only in the Na_2S + Na_2SO_3 sacrificial solution, which is toxic and not stable under air conditions.[15] Unfortunately, sulfide photocatalysts give negligible photocatalytic activity in widely used hole scavengers, such as methanol.[16] If we can fabricate a hetero-nanomaterial composed of ZnO and the sulfide heterostructure, we can simultaneously take the advantages of the two components for photocatalytic water splitting.[17] This material may not only improve the photocatalytic activity of sulfide photocatalysts in the traditional Na_2S + Na_2SO_3 solution, but also make the utilization of methanol solution as the sacrificial reagent for sulfide photocatalysts possible. To date, both the fabrication of fine-grained ZnO-embedded sulfide heterostructures and the search for an efficient method for improving the photocatalytic activity in methanol sacrificial solution have been scarcely reported.

In view of the aforementioned ideas, we select $Zn_{1-x}Cd_xS$/CdS as the sulfide heterostructure to synthesize a ZnO-embedded fine-grained $Zn_{1-x}Cd_xS$/CdS heterostructure using a surfactant-free hydrothermal method based on the following points: (i) $Zn_{1-x}Cd_xS$/CdS shows improved structure matching and photocatalytic performance due to the tunable parameters, as well as the excellent photocatalytic activity of $Zn_{1-x}Cd_xS$;[18] (ii) ZnS precursors with different morphologies were prepared by changing the concentrations of NaOH, and the exposed active site content of the $Zn_{1-x}Cd_xS$/CdS heterostructure could be facilely modulated by the varied particle sizes of the ZnS precursors; (iii) the *in situ* embedding of well-dispersed ZnO nanocrystals on the $Zn_{1-x}Cd_xS$/CdS heterostructure was achieved by the reaction between OH^- and the residual Zn^{2+} derived from the cation exchange of ZnS with Cd^{2+}.

Herein, the $Zn_{1-x}Cd_xS$/CdS heterostructures with modulated morphologies were facilely fabricated through varying the particle sizes of ZnS precursors by implantation of OH^- on their surfaces. The photocatalytic activity of the $Zn_{1-x}Cd_xS$/CdS heterostructures was found to be closely dependent on the exposed active sites, and the heterostructure with the smallest particle size shows the maximal H_2-evolution activity of 22.99 mmol h^{-1} g^{-1}. The *in situ* synthesis of the ZnO-embedded $Zn_{1-x}Cd_xS$/CdS heterostructure was achieved by introducing different amounts of NaOH. The ZnO nanocrystal, serving as a cocatalyst to separate the charge carriers and acting as a H_2-production site, contributes to the tremendous enhancement in the photocatalytic activity of the $Zn_{1-x}Cd_xS$/CdS heterostructure to 84.17 mmol h^{-1} g^{-1}, especially in the methanol solution. Notably, the ZnO-embedded $Zn_{1-x}Cd_xS$/CdS shows a distinct photocatalytic H_2-production rate of 0.18 mmol h^{-1} g^{-1} even in the absence of a sacrificial agent, whereas $Zn_{1-x}Cd_xS$/CdS shows no hydrogen production. The exposed active site content and the loading of the ZnO cocatalyst on the heterojunction show a synergistic effect on the photocatalytic H_2-evolution activity.

Experimental section

Materials

Cadmium nitrate tetrahydrate ($Cd(NO_3)_2{\cdot}4H_2O$), zinc chloride ($ZnCl_2$), thiourea (CH_4N_2S) and sodium hydroxide (NaOH) were of analytical grade and used as-received without further purification.

Synthesis of ZnS precursors with different particle sizes

The ZnS precursors were prepared using $ZnCl_2$ and CH_4N_2S as the Zn and S sources *via* a hydrothermal method. NaOH was adopted to modulate the particle size of ZnS. In a typical process, 3.0 mmol of $ZnCl_2$ and 6.0 mmol of CH_4N_2S were dissolved in 25 mL of distilled water (solution A). Different amounts of NaOH with the molar ratios of NaOH/Zn equal to 0, 1, 2, 4, 8, 10 and 20 were dissolved in 5 mL of distilled water (solution B). Then, solution B was added to solution A slowly under ultrasound for 0.5 h. The resultant solution was subsequently transferred into a 50 mL Teflon-lined autoclave and maintained at 180 °C for 21 h. The final white products were rinsed three times with distilled water and ethanol, respectively, and dried overnight at 60 °C in a vacuum oven to evaporate the solvent. The obtained ZnS nanocrystals with different particle sizes were used as precursors for the fabrication of the heterostructure samples.

Synthesis of the heterostructure samples with morphologies modulated by the different particle sizes of the ZnS precursors

30 mg of ZnS precursors (prepared with molar ratios of NaOH/Zn = 0, 1, 2, 4, 8, 10, 20) were dissolved in 10 mL of deionized water under ultrasound for a few minutes. A suitable amount of $Cd(NO_3)_2{\cdot}4H_2O$ (Cd/(Zn + Cd) = 30 at%) was dissolved in deionized water (2.8 mL) and then dropped into the aforementioned solution quickly under mild stirring. After several minutes, the obtained solution was transferred into a 15 mL autoclave and maintained at 140 °C for 12 h. The final products were rinsed with distilled deionized water and ethanol three times, respectively, and dried overnight at 60 °C in a vacuum oven to evaporate the solvent.

In situ synthesis of the ZnO cocatalyst

30 mg of ZnS with the smallest particle size (prepared with the NaOH/Zn molar ratio of 4) was dissolved in 8 mL of deionized water under ultrasound for a few minutes (solution A). A suitable amount of $Cd(NO_3)_2{\cdot}4H_2O$ (Cd/(Zn + Cd) = 30 at%) was dissolved in deionized water (3 mL) (solution B). Different amounts of NaOH with the ratios of NaOH/Cd equal to 1, 5, 10, 15 and 20 were dissolved in 1 mL of distilled water and then dropped into the mixed solutions of A + B quickly under mild stirring. After several minutes, the obtained solution was transferred into a 15 mL autoclave and maintained at 140 °C for 12 h. The final yellow products were rinsed with distilled deionized water and ethanol three times,

respectively, and dried overnight at 60 °C in a vacuum oven to evaporate the solvent.

Characterization

The powder X-ray diffraction (XRD) patterns were recorded on a D/max 2500 VL/PC diffractometer (Japan) equipped with graphite-monochromatized Cu Kα radiation (λ = 1.54060 Å). The corresponding work voltage and current were 40 kV and 100 mA, respectively. The transmission electron microscopy (TEM) and high-resolution TEM (HRTEM) images were recorded on a JEOL-2100F apparatus at an accelerating voltage of 200 kV. The surface morphologies of the heterojunction materials were examined using a scanning electron microscope (SEM, JSM-7600F) at an accelerating voltage of 10 kV. Energy-dispersive X-ray spectroscopy (EDX) was conducted on a JSM-5160LV-Vantage-type energy spectrometer. UV-vis diffuse reflectance spectra were recorded using a Cary 5000 UV-vis spectrometer (Varian, USA) with $BaSO_4$ as a reflectance standard. The Brunauer–Emmett–Teller (BET) specific surface area (S_{BET}) and nitrogen adsorption of the heterojunction samples were analyzed using an Autosorb-iQ adsorption apparatus (Quantachrome Instruments, USA). All of the samples were degassed at 90 °C for 3 hours prior to nitrogen adsorption measurements. The S_{BET} was determined by a multipoint BET method using the adsorption data in the relative pressure (P/P_0) range of 0.05–0.3. Electrochemical impedance spectra (EIS) measurements were carried out in a three-electrode system and the spectra were recorded over a frequency range of 500 kHz–200 MHz with an AC amplitude of 10 mV at 0.5 V. Na_2S (0.1 M) and Na_2SO_3 (0.02 M) mixture solution was used as the supporting electrolyte. EIS data were recorded using an electrochemical workstation (EC-Lab, SP-150, VMP3-based instruments, America) under a surface power density of about 0.1 mW cm^{-2}. The Raman spectra of the powder samples were obtained on a Lab-RAM HR800 with a laser excitation wavelength of 514.5 nm.

Photocatalytic hydrogen production

The photocatalytic H_2-production experiments were performed *via* a photocatalytic H_2-production activity evaluation system (CEL-SPH2N, CEAULight, China) in a 300 mL Pyrex flask, and the openings of the flask were sealed with a silicone rubber septum. A 300 W xenon arc lamp through a UV-cutoff filter with a wavelength range of 420–1000 nm, which was positioned 13 cm away from the reaction solution, was used as the visible light source to trigger the photocatalytic reaction. The focused intensity on the flask was ~200 mW cm^{-2}, which was measured with an FZ-A visible-light radiometer (CEL-SPH2N, CEAULight, China). In a typical photocatalytic H_2-production experiment, 5 mg of the as-prepared photocatalyst was suspended in 100 mL of a mixed aqueous solution containing Na_2S (0.35 M) and Na_2SO_3 (0.25 M). Before irradiation, the system was vacuumed for 5 min *via* a vacuum pump to completely remove the dissolved oxygen and ensure that the reactor was in an anaerobic environment. A continuous magnetic stirrer was applied at the bottom of the reactor to keep the photocatalyst particles in suspension during the experiments. The H_2 content was analyzed by gas chromatography (GC-7900, CEAULight, China). All glassware was carefully rinsed with distilled water prior to usage.

Results and discussion

$Zn_{1-x}Cd_xS$/CdS heterostructures with adjustable morphologies were accessed by varying the particle sizes of the ZnS precursors.[19] Scheme 1 illustrates the fabrication route for modulating the morphologies of the ZnS precursors, $Zn_{1-x}Cd_xS$/CdS heterostructure and ZnO-embedded $Zn_{1-x}Cd_xS$/CdS heterostructure. The ZnS precursors possessing different particle sizes were firstly fabricated, where the hydroxide plays an indispensable role in the formation of the fine-grained ZnS precursor through the repulsive interaction among ZnS nanoparticles.[20]

The morphologies of $Zn_{1-x}Cd_xS$/CdS heterostructures with the optimal Cd content could be facilely modulated by the different particle sizes of the ZnS precursors (Fig. S1†).[21] The Zn^{2+} ion derived from the cation exchange between ZnS and Cd^{2+} reacted with the superfluous hydroxyl ion and produced $[Zn(OH)_4]^{2-}$, which then immediately transformed into ZnO,[22] and the ZnO-embedded $Zn_{1-x}Cd_xS$/CdS heterostructure was formed. The $Zn_{1-x}Cd_xS$/CdS heterostructure samples derived from the ZnS precursors with different particle sizes were abbreviated as ZAC*m* (*m* = 0, 1, 2, 4, 10, 20; *m* equals to the molar ratio of NaOH/Zn in the preparation of ZnS). As can be observed from the SEM images, the adoption of NaOH leads to the decrease in average diameter of the ZnS nanoparticles from 1.5 μm to around 20 nm (Fig. 1a and b). Significantly, the morphologies of the $Zn_{1-x}Cd_xS$/CdS heterostructure samples were closely dependent on those of the ZnS precursors: the heterostructure derived from ZnS with smaller particle sizes shows a more porous morphology (Fig. 1c and d, Fig. S2†).

Characterization of the phase structure *via* XRD (Fig. 1e) indicates that the modulated morphology of the

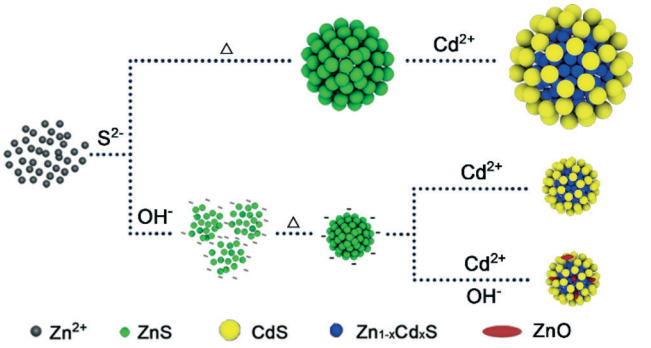

Scheme 1 Schematic illustration of the fabrication of ZnS precursors, $Zn_{1-x}Cd_xS$/CdS heterostructures with modulated morphologies, and the ZnO-embedded $Zn_{1-x}Cd_xS$/CdS heterostructure.

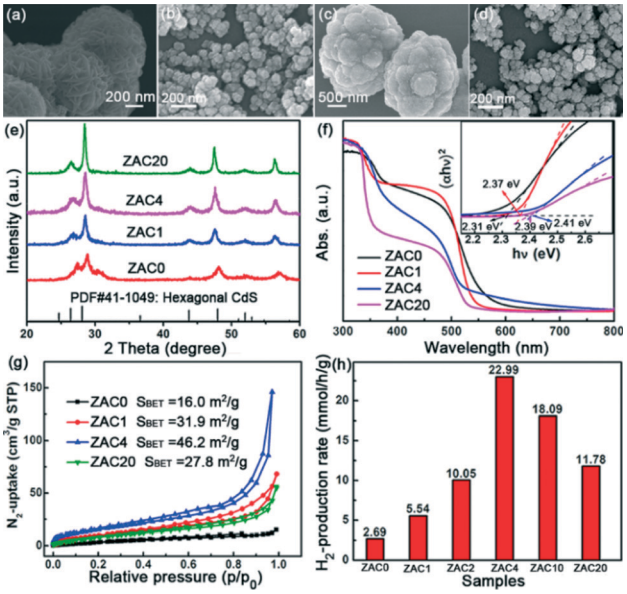

Fig. 1 The SEM images of (a, b) ZnS prepared without and with NaOH (the molar ratio of NaOH/Zn equals 4), and (c, d) the corresponding heterojunction samples. The (e) XRD patterns, (f) UV-vis diffuse reflectance spectra and the corresponding $(\alpha h\nu)^2$ *versus* $h\nu$ curves (inset), and (g) nitrogen adsorption/desorption isotherms of the heterostructure samples with different particle sizes. (h) The H_2-evolution rate of heterojunctions with different particle sizes.

heterostructure samples resulting from the different particle sizes of ZnS shows a tremendous effect on the crystallinity of the heterostructure. Compared with ZAC0, ZAC4 possesses much stronger diffraction peaks corresponding to CdS and $Zn_{1-x}Cd_xS$ phases due to its smaller particle size, and larger heterostructure active site content confirmed by the largest amount of Cd from the EDX results (Fig. S3†). The S, Zn and Cd species distribute uniformly in the whole matrix of the nanoparticles (Fig. S4†). The band structure of the as prepared heterostructure samples was investigated by the UV-vis diffuse reflectance spectra and displayed in Fig. 1f. Notably, the spectra of the heterostructure samples show two band edges, and the entire diffuse reflectance spectra could be divided into regions I and II, which correspond to absorption in the UV and visible regions, respectively.[18] Moreover, the heterostructure samples with smaller particle size possess a larger bandgap (E_g) in region II (inset of Fig. 1f), which may be attributed to the quantum effect of CdS.[18]

A large surface area usually means more surface sites, which could facilitate the adsorption and reaction of reactants and thus increase the photocatalytic activity due to the surface-based characteristic of the photocatalytic water splitting reaction.[23] With decreasing particle size, both ZnS and the relevant heterostructure show much larger nitrogen adsorption volumes and S_{BET} (Fig. S5†) than those prepared without NaOH. Consequently, ZAC4 with the smallest particle size shows the largest nitrogen adsorption volume and S_{BET} among the ZAC*m* samples (Fig. 1g). The HRTEM image of ZAC4 (Fig. S6†) exhibits two lattice fringes with lattice constants of 0.334 and 0.207 nm, which correspond to $Zn_{1-x}Cd_xS$ and CdS, respectively.

The photocatalytic H_2-evolution activities of the heterostructure samples were examined in an aqueous solution containing 0.35 M Na_2S and 0.25 M Na_2SO_3 under visible light irradiation ($\lambda \geq 420$ nm) and are compared in Fig. 1h. The decreased particle size in the ZAC*m* samples results in the enhanced photocatalytic activity, and the maximum H_2-evolution rate as high as 22.99 mmol h^{-1} g^{-1} was obtained in ZAC4. On the other hand, a further increase in the amount of NaOH leads to a slight reduction in the photocatalytic activity of the heterostructures due to their increased particle size. To validate the universality of this method, ZnS/CuS heterostructures with modulated morphologies and optimal Cu content were prepared by adopting ZnS with different particle sizes as precursors.[24] The ZnS/CuS derived from ZnS prepared with a NaOH/Zn ratio of 4 shows much smaller particle size, larger nitrogen uptake and S_{BET}, and much better photocatalytic activity under visible light (Fig. S7†) than the ZnS/CuS derived from ZnS prepared without NaOH.

On the basis of the investigation into the particle size-dependent photocatalytic activity, the optimal ZnS precursor with the smallest particle size was selected for further studying the effect of ZnO on the transfer efficiency of charge carriers and photocatalytic activity of the heterostructure. Different amounts of NaOH were adopted for the *in situ* synthesis of the ZnO-embedded $Zn_{1-x}Cd_xS$/CdS heterostructures. The samples prepared with different NaOH/Cd^{2+} molar ratios (labelled as *n*) were abbreviated as ZACA*n* (*n* = 0, 1, 5, 10, 15 and 20). Compared with ZACA0, the other ZACA*n* samples show much stronger diffraction peaks corresponding to the CdS phase, and obvious diffraction peaks of ZnO were observed (Fig. 2). By comparison of the UV-vis diffuse reflectance spectra of the ZACA*n* samples (Fig. S8†), the adoption of NaOH for the reaction between ZnS and Cd^{2+} shows no effect on the band structure of the heterostructure.

Characterization of the element distribution by element mapping indicates that all the O, S, Zn and Cd elements were

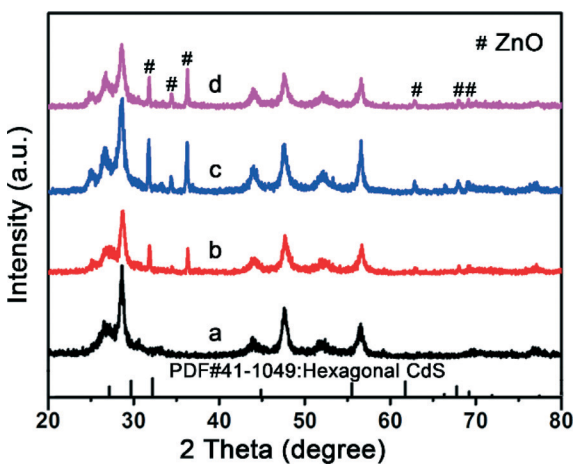

Fig. 2 XRD patterns of the ZnO-embedded $Zn_{1-x}Cd_xS$/CdS heterostructure samples of (a) ZACA0, (b) ZACA1, (c) ZACA10 and (d) ZACA20.

well distributed in the skeleton of the heterostructure samples (Fig. 3a). As can be observed in the TEM image of ZACA10 (Fig. 3b), the nanoparticles show a uniform size distribution with an average diameter of around 20 nm. The ZnO-embedded $Zn_{1-x}Cd_xS$/CdS heterostructure was further confirmed by HRTEM (Fig. 3c). The lattice fringes corresponding to CdS, ZnO and $Zn_{1-x}Cd_xS$ with a well-defined heterostructure can be observed, and CdS quantum dots were loaded on the surface of the $Zn_{1-x}Cd_xS$ nanoparticle core. Moreover, the ordered lattice fringes with the interplanar spacing of 0.282 nm, corresponding to the ZnO nanocrystals, can be observed at the edge of the $Zn_{1-x}Cd_xS$ nanoparticle.

The effect of the ZnO nanocrystals on the photocatalytic activity of the $Zn_{1-x}Cd_xS$/CdS heterostructure is compared in Fig. S9.† The formation of ZnO in the heterostructure could enhance its photocatalytic activity drastically, and ZACA10 possessing the largest amount of ZnO shows the highest photocatalytic activity. Considering the similar microstructure morphology, S_{BET} (Fig. S10†) and band structures of ZACA0 and ZACA10, the improved photocatalytic H_2-evolution rate from 22.99 mmol h^{-1} g^{-1} in ZACA0 (ZAC4) to 84.17 mmol h^{-1} g^{-1} in ZACA10 is mainly attributed to the formation of ZnO. This value is 765 times higher than that of CdS prepared by a hydrothermal method, and is competitive in comparison with the previously reported CdS-based heterostructure (Table S1, ESI†).[5,18,21,25] It is well known that ZnO prepared by a wet chemistry method at low temperature always possesses defects, such as oxygen vacancies, which may facilitate the charge separation and act as hydrogen production sites as reported in previous publications.[26] The oxygen vacancies in ZnO were confirmed by the peak located at around 580 cm^{-1} in the Raman spectra (Fig. S11†).[27] Additionally, the ZnO-embedded heterostructure possesses an excellent photocatalytic lifetime over 40 h (Fig. S12†). Significantly, the photocatalytic stability of the ZnO-embedded $Zn_{1-x}Cd_xS$/CdS heterostructure was further confirmed by the unchanged phase structure of ZACA10 in XRD after visible light irradiation for 40 h (Fig. S13†), which indicates that the stable phase of ZnO loaded closely into the $Zn_{1-x}Cd_xS$/CdS skeleton even in dilute alkaline solution. The charge-carrier separation and transportation efficiencies were further verified *via* the EIS spectra (Fig. S14†). In accordance with the photocatalytic activity, ZACA10 shows the smallest semicircle in the middle-frequency region, which indicates its fastest interfacial charge transmission.[28]

Since the sacrificial solution (Na_2S + Na_2SO_3) for sulfide heterostructures is toxic and not stable during their practical application in air atmosphere, methanol has been employed as the sacrificial agent. The extremely important role of ZnO in the photocatalytic activity has been systematically investigated by comparing the photocatalytic H_2-production of the ZnO-embedded $Zn_{1-x}Cd_xS$/CdS heterostructure (ZACA10) and $Zn_{1-x}Cd_xS$/CdS heterostructure (ZACA0) in different reaction solutions as shown in Fig. 4a. As was previously mentioned, the fine-grained $Zn_{1-x}Cd_xS$/CdS heterostructure possessed excellent photocatalytic activity in the Na_2SO_3 + Na_2S solution, but showed a negligible photocatalytic H_2-evolution rate in methanol solution.[16] Unexpectedly, the presence of ZnO nanocrystals enhanced the photocatalytic activity obviously. Considering that the oxidation process of sacrificial agents is complicated and their oxidation dynamics should be different due to the different pH circumstances and oxidation process, sodium hydroxide has been added to the neutral methanol solution to obtain a similar alkalinity to that of the Na_2SO_3 + Na_2S solution. Also, ZACA10 shows a photocatalytic activity of 55.22 mmol h^{-1} g^{-1} in alkaline methanol solution, which is very competitive in comparison with that in the Na_2SO_3 + Na_2S solution (84.17 mmol h^{-1} g^{-1}). On the other hand, ZACA0 still possesses a very low photocatalytic activity of only 2.35 mmol h^{-1} g^{-1}. The photocatalytic activity of ZACA10 is 23.48 times higher than that of ZACA0 in alkaline methanol solution, which is much larger than that (3.67 times) in the Na_2SO_3 + Na_2S solution. The tremendous distinction may be stemmed from the oxygen vacancies in ZnO, which could facilitate the separation of charge carriers, act as H_2-evolution sites and possess a stronger oxidative capacity.

To further investigate the role of ZnO in improving the photocatalytic activity of the $Zn_{1-x}Cd_xS$/CdS heterostructure, an alkaline solution with the same pH value as that of the Na_2SO_3 + Na_2S solution has been used as the reaction solution for evaluating the photocatalytic activities of ZACA0 and ZACA10.[29] Notably, in contrast to the negligible hydrogen evolution from ZACA0, ZACA10 gives a considerable

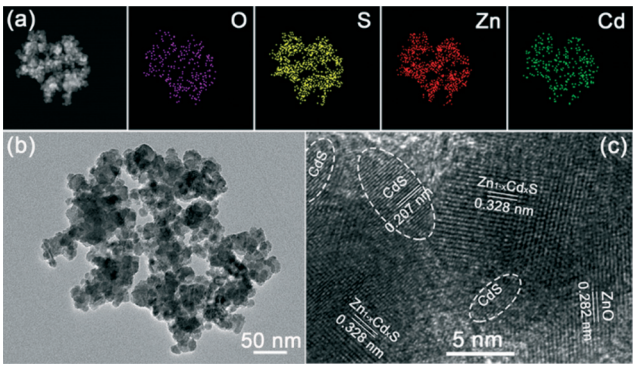

Fig. 3 The (a) element mapping, (b) TEM and (c) HRTEM images of the ZnO-embedded $Zn_{1-x}Cd_xS$/CdS heterostructure.

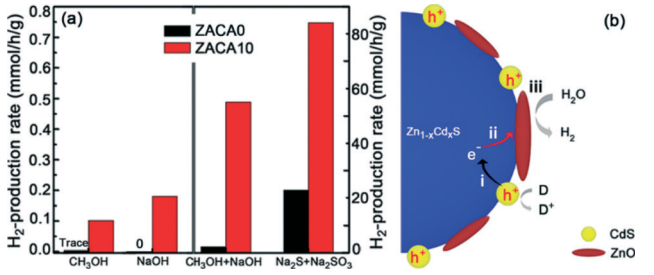

Fig. 4 The (a) comparison results of the photocatalytic activities of ZACA0 and ZACA10 under visible light ($\lambda \geq 420$ nm) in different reaction solutions. The (b) transport of charge carriers in the ZnO-embedded $Zn_{1-x}Cd_xS$/CdS heterostructure.

photocatalytic activity of 0.18 mmol h^{-1} g^{-1} even in the absence of a sacrificial agent. Considering their similar band structure and morphology, this qualitative change comes from the embedding of ZnO nanocrystals in ZACA10. It is well known that the sacrificial agent plays a vital role in the photocatalytic hydrogen evolution by consuming the photogenerated holes and facilitating the separation of charge carriers. Consequently, in the absence of hole scavengers, the $Zn_{1-x}Cd_xS$/CdS heterostructure (ZACA0) without ZnO shows no hydrogen production. Thus, the ZnO cocatalyst can facilitate the separation of charge carriers and act as the hydrogen production site, and hence increase the hydrogen production even without a sacrificial solution.[30] The transfer of the photo-generated charge carriers and electrons in the ZnO-embedded $Zn_{1-x}Cd_xS$/CdS heterostructure can be divided into three steps as shown in Fig. 4b. Under visible light irradiation, the photo-generated electrons transport from the conduction band (CB) of CdS to that of $Zn_{1-x}Cd_xS$ as reported in previous publications,[18] while the photo-generated holes in the valence band (VB) of CdS can be consumed by the sacrificial solution rapidly. In the second step, the electrons are further transferred into ZnO due to its wide E_g, where the electrons are trapped by the oxygen vacancies of ZnO.[30] Finally, ZnO can act as the reaction site for proton reduction and hydrogen production.

Conclusions

In summary, the exposed active site content and morphology of $Zn_{1-x}Cd_xS$/CdS could be facilely modulated by the particle size of the ZnS precursors. By simply increasing its active site content, the photocatalytic activity of the heterostructure increased 8.5-fold in the Na_2SO_3 + Na_2S solution. The photocatalytic H_2-production rate of the $Zn_{1-x}Cd_xS$/CdS heterostructure can be further increased to 84.17 mmol h^{-1} g^{-1} by embedding ZnO as the cocatalyst. Moreover, the existence of ZnO nanocrystals contributes to the competitive photocatalytic activity in methanol in comparison with that in the Na_2S + Na_2SO_3 solution under similar alkaline circumstances. More significantly, the ZnO-embedded $Zn_{1-x}Cd_xS$/CdS heterostructure considerably produces H_2 even without a sacrificial agent, whereas the $Zn_{1-x}Cd_xS$/CdS heterostructure shows no hydrogen evolution. This work not only introduces a facile surfactant-free hydrothermal route for increasing the amount of exposed active sites in heterostructures, but also makes the improved photocatalytic activity of sulfide photocatalysts in eco-friendly sacrificial solution possible.

Acknowledgements

This work was financially supported by NSFC (No. 21371099 and 21471080), the Jiangsu Specially-Appointed Professor, the NSF of Jiangsu Province of China (No. BK20130043 and BK20141445), the Natural Science Research of Jiangsu Higher Education Institutions of China (No. 13KJB150021), the Priority Academic Program Development of Jiangsu Higher Education Institutions, and the Foundation of Jiangsu Collaborative Innovation Center of Biomedical Functional Materials.

Notes and references

1 (*a*) Q. Li, B. Guo, J. Yu, J. Ran, B. Zhang, H. Yan and J. R. Gong, *J. Am. Chem. Soc.*, 2011, **133**, 10878; (*b*) Z. Shen, G. Chen, Q. Wang, Y. Yu, C. Zhou and Y. Wang, *Nanoscale*, 2012, **4**, 2010; (*c*) F. Zuo, K. Bozhilov, R. J. Dillon, L. Wang, P. Smith, X. Zhao, C. Bardeen and P. Feng, *Angew. Chem., Int. Ed.*, 2012, **51**, 6223.

2 X. Zhang, Y. Liu, S.-T. Lee, S. Yang and Z. Kang, *Energy Environ. Sci.*, 2014, **7**, 1409.

3 D. Chen, F. Zhao, H. Qi, M. Rutherford and X. Peng, *Chem. Mater.*, 2010, **22**, 1437.

4 Q. Xiang, B. Cheng and J. Yu, *Appl. Catal., B*, 2013, **138–139**, 299.

5 Y. P. Xie, Z. B. Yu, G. Liu, X. L. Ma and H.-M. Cheng, *Energy Environ. Sci.*, 2014, **7**, 1895.

6 N. Bao, L. Shen, T. Takata and K. Domen, *Chem. Mater.*, 2008, **20**, 110.

7 (*a*) X. Lai, J. E. Halpert and D. Wang, *Energy Environ. Sci.*, 2012, **5**, 5604; (*b*) L. Wang, H. Wei, Y. Fan, X. Liu and J. Zhan, *Nanoscale Res. Lett.*, 2009, **4**, 558.

8 H. McDaniel, M. Pelton, N. Oh and M. Shim, *J. Phys. Chem. Lett.*, 2012, **3**, 1094.

9 X. Xu, L. Hu, N. Gao, S. Liu, S. Wageh, A. A. Al-Ghamdi, A. Alshahrie and X. Fang, *Adv. Funct. Mater.*, 2015, **25**, 445.

10 (*a*) J. Ran, J. Zhang, J. Yu, M. Jaroniec and S. Z. Qiao, *Chem. Soc. Rev.*, 2014, **43**, 7787; (*b*) J.-H. Kang, S. H. Kim, M. Ebaid, J. K. Lee and S.-W. Ryu, *Acta Mater.*, 2014, **79**, 188; (*c*) Q. Xiang, J. Yu and M. Jaroniec, *J. Am. Chem. Soc.*, 2012, **134**, 6575.

11 (*a*) C. Eley, T. Li, F. Liao, S. M. Fairclough, J. M. Smith, G. Smith and S. C. E. Tsang, *Angew. Chem., Int. Ed.*, 2014, **53**, 7838; (*b*) X. Wang, G. Liu, Z.-G. Chen, F. Li, L. Wang, G. Q. Lu and H.-M. Cheng, *Chem. Commun.*, 2009, 3452; (*c*) S. R. Lingampalli, U. K. Gautam and C. N. R. Rao, *Energy Environ. Sci.*, 2013, **6**, 3589; (*d*) Y. Tak, S. J. Hong, J. S. Lee and K. Yong, *J. Mater. Chem.*, 2009, **19**, 5945.

12 (*a*) Y. Tang, H. Zhou, K. Zhang, J. Ding, T. Fan and D. Zhang, *Chem. Eng. J.*, 2015, **262**, 260; (*b*) C. Wang, D. Wu, P. Wang, Y. Ao, J. Hou and J. Qian, *Appl. Surf. Sci.*, 2015, **325**, 112.

13 G. R. Li, T. Hu, G. L. Pan, T. Y. Yan, X. P. Gao and H. Y. Zhu, *J. Phys. Chem. C*, 2008, **112**, 11859.

14 J. Hu, Y. Fan, Y. Pei, M. Qiao, K. Fan, X. Zhang and B. Zong, *ACS Catal.*, 2013, **3**, 2280.

15 Z. Sun, H. Zheng, J. Li and P. Du, *Energy Environ. Sci.*, 2015, **8**, 2668.

16 K. Wu, Z. Chen, H. Lv, H. Zhu, C. L. Hill and T. Lian, *J. Am. Chem. Soc.*, 2014, **136**, 7708.

17 T.-T. Zhuang, Y. Liu, M. Sun, S.-L. Jiang, M.-W. Zhang, X.-C. Wang, Q. Zhang, J. Jiang and S.-H. Yu, *Angew. Chem., Int. Ed.*, 2015, **54**, 11495.

18 J. Yu, J. Zhang and M. Jaroniec, *Green Chem.*, 2010, **12**, 1611.
19 (*a*) Y. Yu, J. Zhang, X. Wu, W. Zhao and B. Zhang, *Angew. Chem., Int. Ed.*, 2012, **51**, 897; (*b*) Y. Huang, Y. Xu, J. Zhang, X. Yin, Y. Guo and B. Zhang, *J. Mater. Chem. A*, 2015, **3**, 19507.
20 (*a*) J. Zhang, Z. Lin, Y. Lan, G. Ren, D. Chen, F. Huang and M. Hong, *J. Am. Chem. Soc.*, 2006, **128**, 12981; (*b*) D. Li, M. B. Muller, S. Gilje, R. B. Kaner and G. G. Wallace, *Nat. Nanotechnol.*, 2008, **3**, 101.
21 K. Li, R. Chen, S.-L. Li, M. Han, S.-L. Xie, J.-C. Bao, Z.-H. Dai and Y.-Q. Lan, *Chem. Sci.*, 2015, **6**, 5263.
22 (*a*) X. Zou, P.-P. Wang, C. Li, J. Zhao, D. Wang, T. Asefa and G.-D. Li, *J. Mater. Chem. A*, 2014, **2**, 4682; (*b*) E. Mosayebi, S. Azizian and A. Hajian, *Superlattices Microstruct.*, 2015, **81**, 226.
23 F. Chang, J. Luo, X. Wang, Y. Xie, B. Deng and X. Hu, *J. Colloid Interface Sci.*, 2015, **459**, 136.
24 J. Zhang, J. Yu, Y. Zhang, Q. Li and J. R. Gong, *Nano Lett.*, 2011, **11**, 4774.
25 (*a*) Q. Li, H. Meng, P. Zhou, Y. Zheng, J. Wang, J. Yu and J. Gong, *ACS Catal.*, 2013, **3**, 882; (*b*) G. Xin, B. Yu, Y. Xia, T. Hu, L. Liu and C. Li, *J. Phys. Chem. C*, 2014, **118**, 21928; (*c*) Q. Wang, J. Li, Y. Bai, J. Lian, H. Huang, Z. Li, Z. Lei and W. Shangguan, *Green Chem.*, 2014, **16**, 2728; (*d*) Z. Han, G. Chen, C. Li, Y. Yu and Y. Zhou, *J. Mater. Chem. A*, 2015, **3**, 1696; (*e*) J. Zhang, Y. Wang, J. Jin, J. Zhang, Z. Lin, F. Huang and J. Yu, *ACS Appl. Mater. Interfaces*, 2013, **5**, 10317; (*f*) L. Huang, X. Wang, J. Yang, G. Liu, J. Han and C. Li, *J. Phys. Chem. C*, 2013, **117**, 11584.
26 (*a*) H.-L. Guo, Q. Zhu, X.-L. Wu, Y.-F. Jiang, X. Xie and A.-W. Xu, *Nanoscale*, 2015, **7**, 7216; (*b*) B. Sambandam, R. J. V. Michael and P. T. Manoharan, *Nanoscale*, 2015, **7**, 13935.
27 (*a*) C. W. Zou, F. Liang and S. W. Xue, *Appl. Surf. Sci.*, 2015, **353**, 1061; (*b*) Q. Huang, T. X. Cun, W. B. Zuo and J. P. Liu, *Appl. Surf. Sci.*, 2015, **332**, 581; (*c*) Y. W. Tang, H. Zhou, K. Zhang, J. Ding, T. X. Fan and D. Zhang, *Chem. Eng. J.*, 2015, **262**, 260.
28 J. Zhang, J. Yu, M. Jaroniec and J. R. Gong, *Nano Lett.*, 2012, **12**, 4584.
29 (*a*) T. Simon, N. Bouchonville, M. J. Berr, A. Vaneski, A. Adrović, D. Volbers, R. Wyrwich, M. Döblinger, A. S. Susha, A. L. Rogach, F. Jäckel, J. K. Stolarczyk and J. Feldmann, *Nat. Mater.*, 2014, **13**, 1013; (*b*) F. T. Wagner and G. A. Somorjai, *Nature*, 1980, **285**, 559.
30 S. Polarz, J. Strunk, V. Ischenko, M. W. E. van den Berg, O. Hinrichsen, M. Muhler and M. Driess, *Angew. Chem., Int. Ed.*, 2006, **45**, 2965.

